Journal of Advanced Ceramics
2012, 1(2): 110-129
DOI: 10.1007/s40145-012-0009-x ISSN 2226-4108

Review

Some recent studies on glass/glass-ceramics for use as sealants with special emphasis for high temperature applications

G. P. Kothiyal[a,*], Madhumita Goswami[a], Babita Tiwari[b], Kuldeep Sharma[a,c], A. Ananthanarayanan[a,c], Lionel Montagne[c]

[a]*Glass and Advanced Ceramics Division, Bhabha Atomic Research Centre, Mumbai-400085, India*
[b]*Technical Physics Division, Bhabha Atomic Research Centre, Mumbai-400085, India*
[c]*Université Lille Nord de France, UCCS - Unité de Catalyse et Chimie du Solide – UMR CNRS 8181, Ecole Nationale Supérieure de Chimie de Lille, Université des Sciences et Technologies de Lille, BP 108, 59562 Villeneuve d' AscqCedex, France*

Received March 26, 2012; Accepted April 5, 2012

Abstract: Glass-ceramics owing to a combination of useful properties such as tuneable thermal expansion coefficient (TEC), good mechanical durability and chemical inertness find widespread uses in a variety of applications including seals and coatings. Glass-ceramic-to-metal seals have been fabricated with various silicate, phosphate and borate based oxide glasses depending upon the intended application. In this article, we review our studies on various glass and glass-ceramics materials development with a view to understand bonding behaviour with metals/alloys at ambient and high temperatures through a comprehensive structure property correlation investigations. Detail studies on BaO-CaO-Al_2O_3-B_2O_3-SiO_2 (BCABS), barium strontium alumino-silicate, and strontium alumino-silicate with different additives (like Nd_2O_3, La_2O_3, NiO, TiO_2, V_2O_5, ZrO_2, Cr_2O_3, and P_2O_5) and barium/strontiun zinc silicate (B/SZS) glass-ceramics for high temperature sealing. We shall illustrate the role of various thermo-physical and structural characterization techniques that allowed optimum selection of materials and processing parameters. We particularly highlight the complementary role of NMR and XRD in studying the material at the short range and long range length scales.

Key words: crystallization; sintering; glass-ceramics; solid oxide fuel cells; NMR

1 Introduction

Glass-ceramics are a kind of polycrystalline materials formed by controlled crystallization of parent glasses [1-4]. These materials consist of polycrystalline regions 'growing' in a matrix of residual glass [5]. Glass-ceramics display a large number of useful properties that include high chemical durability, resistance to thermal and mechanical shocks and the possibility of tuneable thermal expansion coefficient (TEC) [6-8]. As a result, glass-ceramics find wide ranging application in cookware, telescope mirror

* Corresponding author.
E-mail: gpkoth@barc.gov.in

supports, hermetic sealing, etc [9-12]. The thermo-physical properties of glass-ceramics are a function of not only the composition but also the crystallization heat treatment. Therefore, for various applications, the compositions, nucleating agents (to crystallize the desired phases) and heat treatments must be judiciously optimized to obtain materials with the necessary thermo-physical properties. In this article we review sealing of glass-to-metal/alloy and glass-ceramics-to-metal/alloy with a focus on some recent sealing glass-ceramic development [1-3,11-13]. One of the recent applications of glass-ceramics, which places great demand on materials performance, is sealing of solid oxide fuel cells (SOFCs) using glass/glass-ceramics, to effectively channel fuel and oxidant (commonly air) [14-20]. SOFC based power generation presents many advantages, including higher efficiency, lower environmental impact and ability to co-generate heat from the exhaust gas to name a few, as compared to conventional power generation [21-28]. The glass-ceramics used for sealing must show good matching of thermal expansion coefficient (TEC) with other SOFC components, low reactivity with other fuel cell components and long term stability at elevated temperature in either oxidizing or wet reducing atmosphere [21,29,30-33]. Achieving a sealant that fulfils these conditions is important to long term stability of SOFC stacks. Most SOFC sealants reported so far have been based on the alkaline earth alumino-silicate system such as barium alumino-silicate due to good thermal expansion matching and the ability to wet materials such as the interconnect allowing good sealing [21,29,30,31,33,34]. While the chemical durability of these glass-ceramics is generally good, it is necessary to further improve phase stability, crystallization behaviour and adhesion behaviour of the glass-ceramics with other SOFC components. Therefore, it is of interest to study the effect of various additives such as TiO_2 (BCABS-T), ZrO_2(BCABS-Z), Cr_2O_3 (BCABS-Cr), and P_2O_5 (BCABS-P) in the BaO-CaO-Al_2O_3-B_2O_3-SiO_2 (BCABS) system in order to tune viscosity, crystallization and adhesion behaviour. The effect of these additives on thermo-physical and structural properties was studied using micro-hardness (MH) measurements, thermo-mechanical analysis (TMA), differential thermal analysis (DTA), scanning electron microscopy (SEM), magic angle spinning nuclear magnetic resonance (MAS-NMR) spectroscopy and sealing studies. Seals fabricated were tested for prolonged periods in simulated SOFC conditions and material performance was evaluated.

Based on preliminary studies, further investigations were carried out to evaluate the effect of systematic addition of P_2O_5 to the BCABS and evaluate the attendant effects of this on structure property correlations using MAS-NMR, SEM, sealing studies and sintering studies using hot stage microscopy (HSM). The role of P_2O_5 and the optimum quantity necessary for sealing are discussed in light of the various experiments carried out on these materials. In addition to these, we also discuss studies carried out on potential SOFC sealants belonging to the barium/ strontiun zinc silicate (B/SZS) glass-ceramic system. In order to limit the size of the article, we focus upon the materials themselves and do not discuss the details of sealing, which is beyond the scope of this article. We direct the reader to the excellent monograph by Donald [4] for further details on the science of sealing. The present article is laid out as follows.

Glass-ceramics as SOFC sealants: (a) Effect of various additives in the BCABS system, (b) Effect of P_2O_5 on structure, thermo-physical and sealing properties of BCABS glasses, (c) Sealants based on barium/strontiun zinc silicate (B/SZS) glass-ceramics, (d) Crystallization kinetics of SZS glasses, (e) Effect of various additives in the SZS system.

All the glasses discussed in this paper have been prepared by the melt quench technique followed by annealing to relieve the thermal stresses and ceramized by controlled heat treatment [2,13]. We briefly mention the preparation technique of each material during the relevant discussion.

2 Effect of various additives in the BCABS system

Driven by the need for acceptable degradation behaviour in wet reducing and oxidizing environments, alkaline earth-boro-silicate based glasses are widely accepted as the choice for SOFC sealing [34-36]. However, long term stability, the interaction behaviour and wetting properties of the sealant with various SOFC components must be optimized. Therefore, various additives have been incorporated into the glasses and their attendant effects on thermo-physical physical properties have been evaluated. The structural changes responsible for these have been studied using a combination of TMA, XRD and SEM. The basic

composition is an alkaline earth silicate alumino-silicate glass with various additives, which can be expressed as 35BaO-15CaO-5Al_2O_3-8B_2O_3-35SiO_2-2M (where M=P_2O_5, Cr_2O_3, TiO_2 or ZrO_2).

The B_2O_3/SiO_2 ratio of the glasses prepared was 0.22, which falls in the required range for good wetting behaviour with interconnect materials and 8YSZ electrolyte [37]. BaO and CaO have been added to reduce the glass transition temperature and allow softening at a low enough temperature to allow sealing. Al_2O_3 has been incorporated into the glasses in order to enhance glass stability during melt quenching as described in the literature [38].

Annealed glass samples were used for thermo-mechanical analysis in order to evaluate the thermal expansion coefficient, glass transition temperature and the dilatometric softening temperature (T_{ds}). The crystallization behaviour of the glasses was studied using DTA, the details of which are reported by us elsewhere [1,3,13,39].

Table 1 summarizes the thermo-physical properties of the glasses prepared. All the glasses prepared showed T_g values in the range of 600 ℃ to 635 ℃, with TEC in the range of 11×10^{-6}/℃ to 13×10^{-6}/℃, indicating their suitability as sealant materials. The DTA curves for the samples are depicted in Fig. 1. The base glass (*sans* additives) and those with additives as well show no pronounced exothermic behaviour indicating slow crystallization kinetics. The only exception is the BCABS-Cr sample, which exhibits a strong exotherm at ~725 ℃. The glass transition temperatures extracted from the DTA curves are in good agreement with those obtained from TMA. This would seem to indicate that particle migration for crystallization is easier in the Cr_2O_3 containing glasses, which is consistent with its role as a network modifier [36]. However, this also means that the conductivity of this sample is the highest as shown in the Arrhenius plot presented in Fig. 2. Also evident in Fig. 2 is a decrease in activation energy for conduction in this sample above 650 ℃, which is within the acceptable range for SOFC application.

The main motive behind the inclusion of additives was that the base glass shows poor interaction with 8YSZ ceramic (Fig. 3a). Figure 3b shows the BCABS-P interface with 8YSZ. The interface appears continuous and a reaction zone is evident indicating intimate interaction between the BCABS-P glass and the 8YSZ ceramic. Similar continuous interfaces were

Table 1 Thermo-mechanical parameters for BCABS glass samples with various additives

Samples	TEC (30-500)× 10^{-6}/℃	T_g (℃)	T_d (℃)	Microhardness (GPa)
BCABS (without substituent)	11.9	619	665	5.68
BCABST	11.58	629	669	5.60
BCABSP	12.04	641	660	5.39
BCABSZ	12.81	652	670	5.74
BCABSCr	11.34	632	678	–

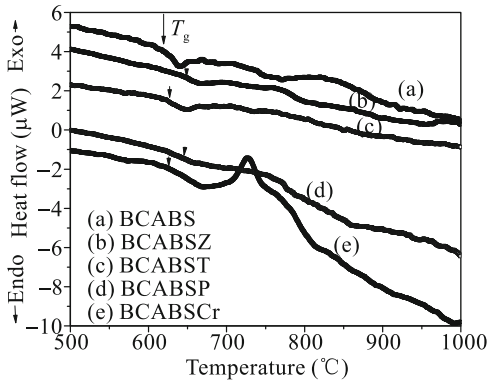

Fig. 1 TA plots of BCABS glasses containing different additives

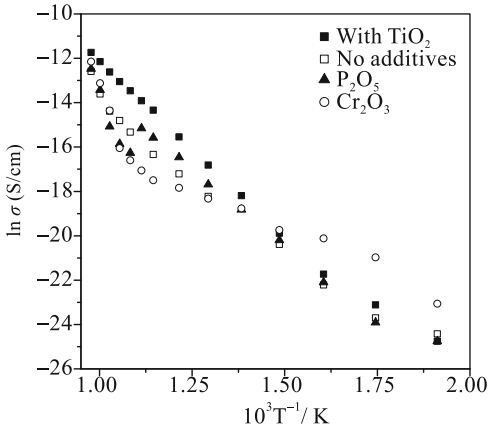

Fig. 2 Arrhenius plot for BCABS glasses containing different additives

observed in case of BCABS-Cr and BCABS-T samples. However, in case of the BCABS-Z samples, the glass shows poor interaction behaviour with the 8YSZ ceramic and the overall wettability is unsatisfactory as evident in Fig. 3d. A more detailed study of the element diffusion profiles for these materials is discussed in a separate publication. Therefore, we conducted further interaction studies with Crofer-22 APU alloy using only BCABS-P, BCABS-Cr and BCABS-T samples.

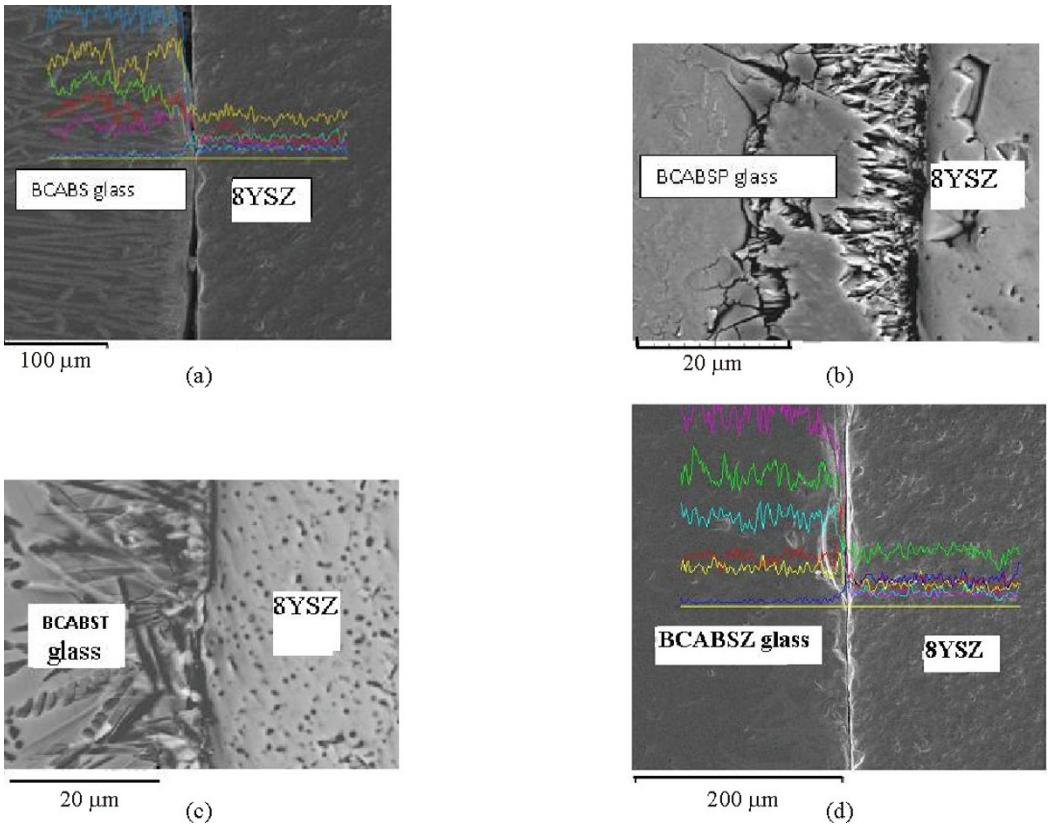

Fig. 3 Microstructure at the interfaces of BCABS glass samples with 8YSZ electrolyte with (a) BCABS, (b) BCABS-P, (c) BCABS-Cr and (d) BCABS-T

Figures 4a, 4b and 4c show the interfaces of BCABS-P, BCABS-Cr and BCABS-T glasses bonded with Crofer-22 APU alloy interconnect materialand and heat treated at 775 ℃ for 300 h. The temperature was chosen using high temperature optical microscopy. In all cases, a continuous interface is clearly evident. The formation of a Cr rich layer about 3-5 μm thick is also evident in these micrographs. We shall demonstrate that in case of the BCABS-P glass-ceramics, this layer could help bonding the glass-ceramic to the metal.

The phase emergence in BCABS-P, BCABS-Cr and BCABS-T after heat treating at 775 ℃ for 300 h is presented in Fig. 5. In case of the BCABS-P sample, the phases formed are a mixture of $Ba_3(PO_4)_2$ and $Ba_2Al_2Si_2O_8$. This latter phase undergoes a polymorphic transition near 300 ℃ accompanied nearly 4% change in volume and can present problems with seal integrity under thermal cycling [41]. Therefore we have carried out an optimization study to evaluate the amount of P_2O_5 that can be added to the BCABS glasses which we present subsequently. In case of BCABS-Cr, $BaCrO_4$ is evident in addition to the other phases and the high TEC of this phase can be detrimental to seal integrity as well. Of the materials studied, TiO_2 incorporation shows the best combination of phases formed with a $Ba_{1.55}Ca_{0.45}SiO_4$ and $BaSi_2O_5$. The thermo-physical properties of these glass-ceramics are collated in Table 2.

Despite the formation of phases that can cause problems with seal integrity, BCABS-P and BCABS-Cr samples remained hermetic even after holding at 775 ℃ for upto 300 h. Since the conductivity of the Cr_2O_3 sample is higher, we decided to investigate further the potential of P_2O_5 as an SOFC sealant.

Table 2 Thermal expansion coefficient as a function of dwell time at 775 ℃ for BCABS samples with different substituents

Sample	Base glass	10 h	100 h	300 h
	TEC(30-300)×10^{-6}/℃			
BCABST	11.34	11.59	11.67	11.02
BCABSP	11.85	11.82	11.43	10.96
BCABS Cr	10.94	11.62	10.95	10.94

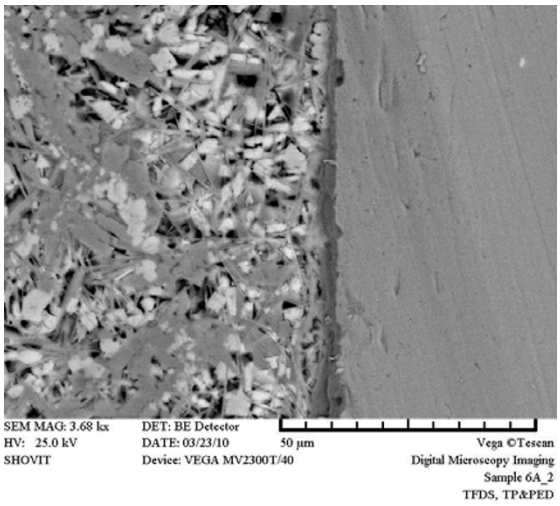

(a)

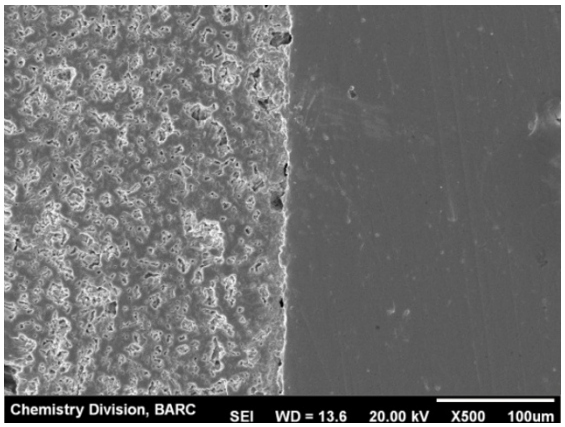

(b)

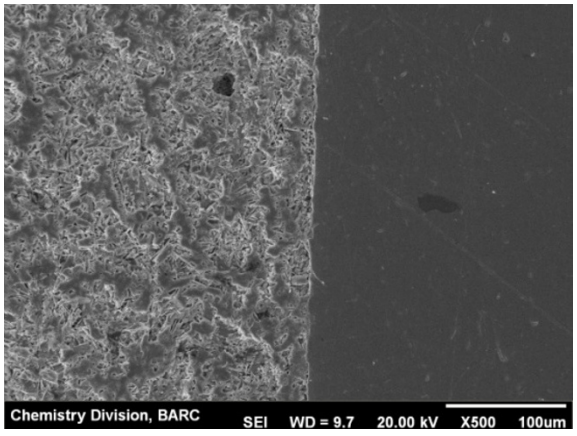

(c)

Fig. 4 Microstructure of the interfaces of BCABS glass samples bonded with Crofer 22 APU and heat treated at 775 ℃ for 300 h; (a) BCABS-P, (b) BCABS-Cr and (c) BCABS-T

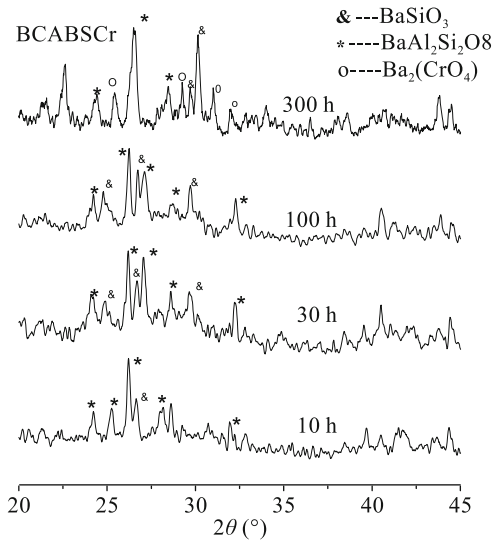

(a)

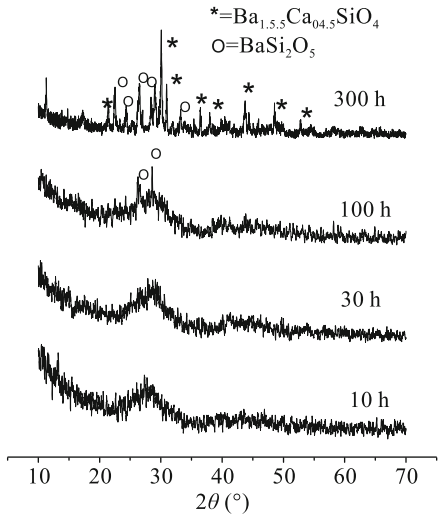

(b)

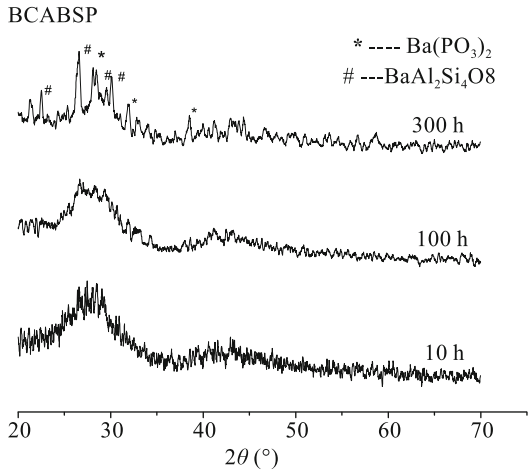

(c)

Fig. 5 Phase emergence in (a) BCABS-P, (b) BCABS-Cr and (c) BCABS-T after heat treatment at 775 ℃ for 300 h

3 Effect of P_2O_5 on structure, thermo-physical and sealing properties of BCABS glasses

In order to investigate the effect of P_2O_5 on the structure and thermo-physical properties of the BCABS glasses, glasses with the general composition $35BaO\text{-}15CaO\text{-}5Al_2O_3\text{-}8B_2O_3\text{-}(35\text{-}x)SiO_2\text{-}xP_2O_5$ were prepared ($0 \leqslant x \leqslant 5$). The samples are nomenclature BCABS-*x*P where *x* is the molar percentage of P_2O_5 incorporated. The thermo-physical properties of the parent glasses prepared by melt quenching and subsequent annealing are presented in Table 3. The T_g values of the parent glasses are observed to increase slightly with P_2O_5 incorporation. T_{ds} is also augmented by P_2O_5 incorporation with a large increase observed for 5 mol% P_2O_5 incorporation. The TEC of the parent glasses reduces slightly till BCABS-4P. However, the TEC of BCABS-5P is significantly lower than the other glasses.

The DTA traces of the samples are presented in Fig. 6. All samples show a glass transition at ~635 ℃, and a broad crystallization exotherm centred on 730 ℃. In addition, the samples BCABS-0P and BCABS-4P show a second broad exotherm around 850 ℃ and 875 ℃ respectively. The crystallization behaviour observed with DTA did not show significant changes with increasing P_2O_5 concentration.

The variation in the thermo-physical properties of the glasses is attributed to increasing polymerization of the silica species as observed in the ^{29}Si NMR spectra presented in Fig. 7. The addition to P_2O_5 removes alkaline earth cations from the silicate network for charge compensation according to Eq. (1).

Table 3 Thermo-Physical properties of BCABS glasses and glass-ceramics (GC)

	CTE×10^{-6} ℃$^{-1}$ (±5%)	T_g±2 (℃)	T_{ds}±2 (℃)
BCABS-0P	11.8	635	674
BCABS-0P GC	12.5	597	875
BCABS-1P	11.6	638	673
BCABS-1P GC	12.2	593	897
BCABS-2P	11.5	641	675
BCABS-2P GC	11.8	622	896
BCABS-3P	11.4	642	677
BCABS-3P GC	12.1	604	923
BCABS-4P	11.2	646	677
BCABS-4P GC	12.3	602	928
BCABS-5P	9.9	653	683
BCABS-5P GC	11.3	607	943

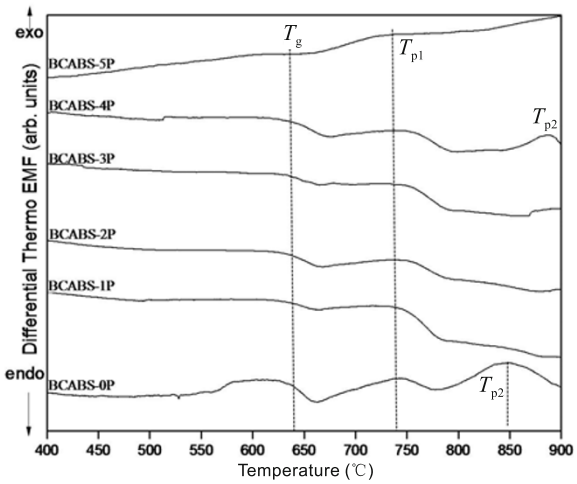

Fig. 6 DTA curves of BCABS glasses containing 0-5 mol% P_2O_5 (bottom to top)

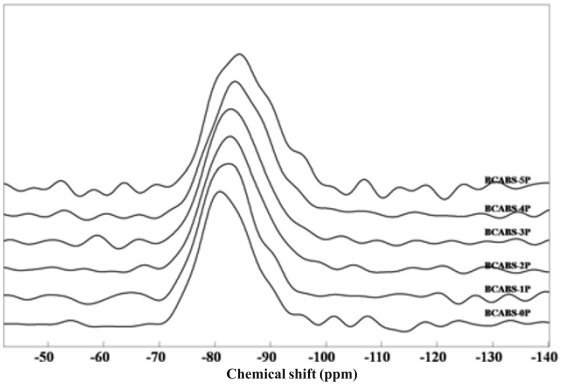

Fig. 7 ^{29}Si MAS-NMR spectra of BCABS-0P to 5P glasses. Note the increasing network polymerization of the glasses with P_2O_5.

$$P_2O_5+6MO \rightarrow 2M_3PO_4 \quad (1)$$

where M=Ba, Ca

Simultaneously, the incorporation of P_2O_5 converts BO_3 structural units into BO_4^- according to the following reaction [30].

$$6B\text{Ø}O_2^{2-}+P_2O_5 \rightarrow 6B\text{Ø}_4^-+2PO_4^{3-} \quad (2)$$

where Ø denotes bridging oxygen. This leads to an increase in the relative BO_4 fraction as observed in ^{11}B MAS-NMR spectra (Fig. 8). Since the glasses have large fractions of modifying cations, these can charge compensate both the PO_4^{3-} and $B\text{Ø}_4^-$ anions. The relative increase of the more rigidly bonded, tetrahedral BO_4 units as compared to the planar BO_3 units also contributes to increased flow temperature, reduced TEC and increased T_g for parent glasses.

It may be emphasized that the modifier cations required for reactions 1 and 2 are removed predominantly from the silicate network. As a result,

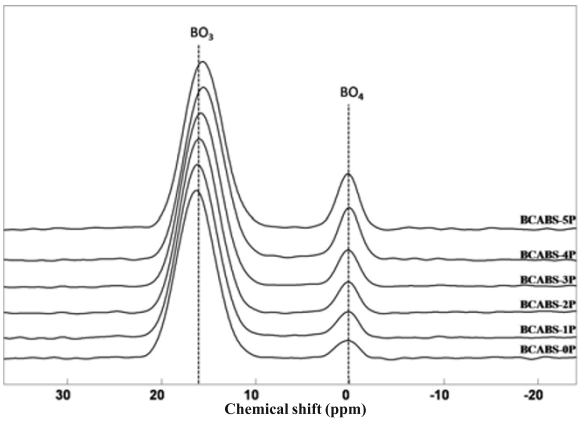

Fig. 8 ^{11}B MAS-NMR spectra of BCABS-0P to 5P glasses

the Al coordination remains primarily tetrahedral (Fig. 9). However, the $Al^{(4)}$ resonance is systematically displaced to lower chemical shift values with increasing P_2O_5. The shift can be attributed to changes in the silicate network polymerization which can cause a change in the Al second neighbour coordination sphere. In addition, this can also be attributed to AlO_4 being increasingly charge compensated by Ba^{2+} (field strength 0.26) instead of Ca^{2+} (field strength 0.36), since the latter would be preferred for charge compensation of PO_4^{3-} units [40]. However, we expect the polymerization change in the silicate network to be the dominant contributor for the displacement of the Al resonance.

Since sealing requires high densification of the glass upon sintering, maximum shrinkage must be attained before the beginning of crystallization. With increasing P_2O_5 fraction, crystallization becomes more prevalent, thus reducing the maximum shrinkage

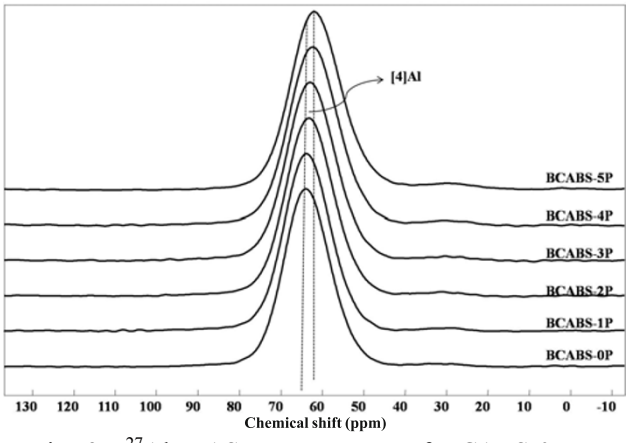

Fig. 9 ^{27}Al MAS-NMR spectra of BCABS-0P to 5P glasses exhibiting Al in tetrahedral coordination

attainable as seen by Hot Stage Microscopy (HSM) experiments [41]. This also leads to a plateau in normalized area prior to sample melting, followed by a sharp reduction in normalized area at the flow temperature, which is typical of the melting of crystalline materials [41]. The poor sintering property of BCABS-4P and 5P, combined with relatively high flow temperature means that sealing to Crofer-22 APU with these compositions would be difficult. It is also interesting to observe that the greatest shrinkage is observed for sample BCABS-2P and that the reduction in shrinkage is marked between BCABS-3P and 4P. This would indicate that at and beyond 3 mol % P_2O_5 incorporation, crystalline phosphate phase separation occurs, as was also observed in borosilicate and alumino borosilicate glasses, which seems to hinder further shrinkage of the samples. This observation is supported by X-Ray diffractograms (Fig. 10) and ^{31}P MAS NMR (Fig. 11) that reveal the formation of $Ba_3(PO_4)$ phase in glass-ceramics containing more than 2 mol % P_2O_5.

Since the incorporation of P_2O_5 removes alkaline earth cations according to reaction (1), the effective glass composition shifts towards the hexacelsian forming region of the barium aluminum silicate phase diagram. As a result, the major phase formed changes from $BaSiO_3$ to a mixture of hexacelsian, calcium/ barium phosphates and barium aluminum oxide. MAS-NMR spectra of the glass-ceramics are in accordance with the phase emergence observed by XRD. However, there is no crystalline resonance on the ^{29}Si spectra of the glass-ceramics (Fig. 12a) corresponding to hexacelsian. This is attributed to the presence of significant Al-Si disorder in hexacelsian similar to other feldspar family minerals [42]. Interestingly, while ^{29}Si NMR spectra do not show any narrow resonance, the ^{27}Al spectra (Fig. 12b) show narrowing attributed to crystallization of hexacelsian and mainly barium aluminum oxide that contain Al in tetrahedral coordination. This could perhaps be due to a greater fraction of the total Al in the glass being involved in the crystalline phases as compared to Si.

The crystallization of phosphate containing phases observed in XRD allows BCABS-4P and 5P glass-ceramics to have high TEC despite the crystallization of hexacelsian, which a lower than desired TEC (8×10^{-6}/℃). The large fraction of aluminium-rich crystalline phases in these glass-ceramics means that the residual glass is enriched in silica and these consequently have higher T_g. Since thermal stresses

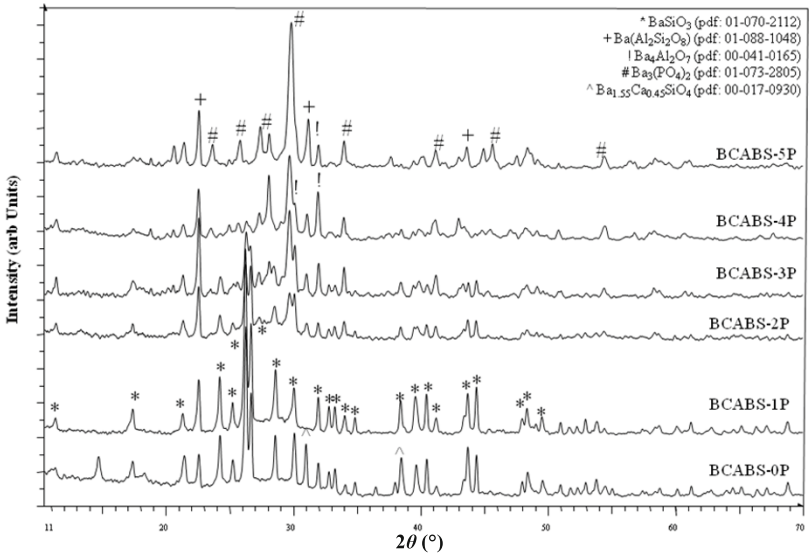

Fig. 10 XRD patterns recorded at room temperature for BCABS-0P to 5P glass-ceramics formed by heat treating BCABS glasses according to the schedule described in the text. The phases formed are indicated in the diagram on the top right corner.

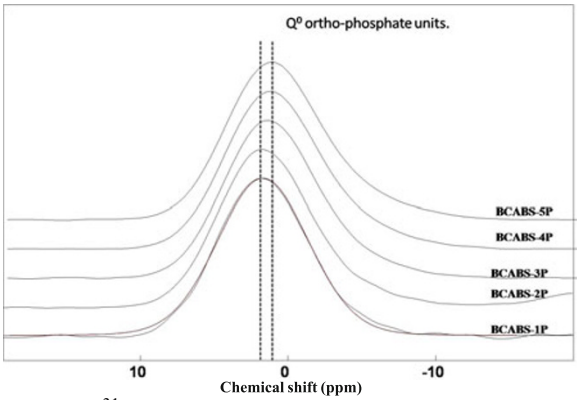

Fig. 11 ^{31}P MAS-NMR spectra of BCABS-0P to 5P glasses

develop below T_g, this can render these materials vulnerable to cracking under thermal cycling. Similarly, BCABS glass-ceramics with low P_2O_5 content show crystallization of $BaSiO_3$, and thus also display a reduction in T_g due to removal of SiO_2 from the residual glassy phase.

Since the flow and sealing temperatures increase with P_2O_5, interface studies were carried out using BCABS-0P, 1P and 2P glasses, as these could be sealed to Crofer-22APU alloy below 1000 ℃. With increasing P_2O_5, dendrites of $BaSiO_3$ (confirmed by WDX analysis) are more uniformly distributed in the bulk of the glass-ceramic, which gives superior properties compared to surface crystallization. However, as

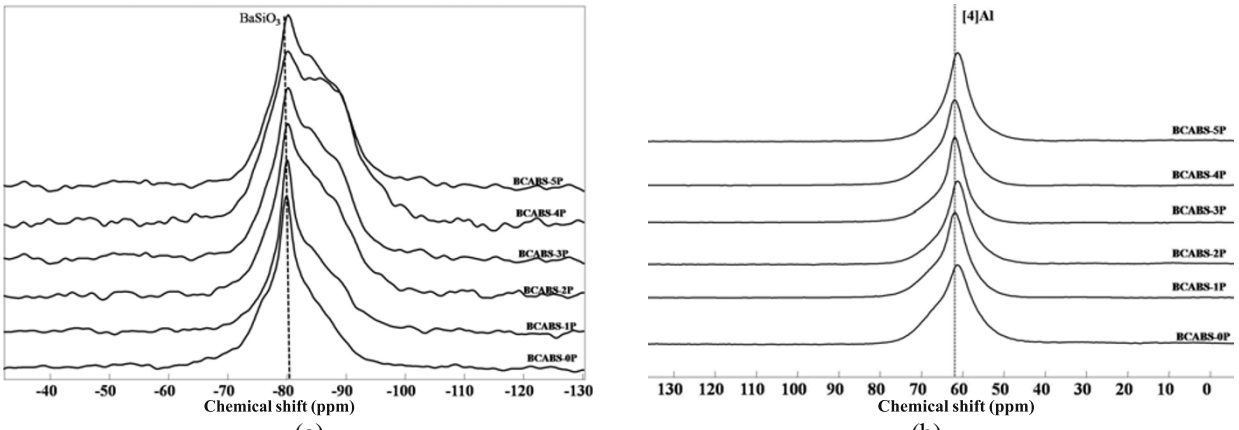

Fig. 12 (a) 29Si MAS-NMR spectra of BCABS-0P to 5P glass-ceramics. In the glass- ceramics, the crystalline resonance at c.a. −80 ppm is attributed to BaSiO3. Ba(Al2Si2O8) does not present a narrow crystalline resonance due to Al-Si disorder. (b) 27Al MAS-NMR spectra of BCABS-0P to 5P glass-ceramics exhibiting Al in tetrahedral coordination although the resonances are narrower indicating the onset of crystalline ordering.

discussed previously, it also interferes with densification upon sintering.

Although the quantity of P_2O_5 in the samples is small, making detection difficult, comparing the P map of glass-ceramics remote from and proximal to the interface seems to indicate a depletion of P_2O_5 near the interface as shown in Fig. 13. This figure represents the WDX images of BCABS-1P but similar behaviour is observed in case of BCABS-2P. Based upon the data, we can tentatively suggest that the P_2O_5 at the interface reacts with the Cr according to the following reactions [4]:

$$Cr^{-}+3/10P_2O_5 \rightarrow 1/2Cr_2O_3+3/5P\uparrow \quad (3)$$

$$Cr^{-}+1/5P_2O_5 \rightarrow CrO+2/5P\uparrow \quad (4)$$

On the basis of the Cr and P maps, it is not possible to conclude whether Reaction (3) or (4) is predominant. However, both reactions result in the formation of P vapors that must leave pores in the glass at the interface. We were unable to observe any such pores at the interface in the BSE images (Fig. 14h for example) [39] and postulate that the pores might be closed near the sealing temperature owing to the fluidity of the glass at elevated temperatures. While further studies are necessary to determine the redox reactions

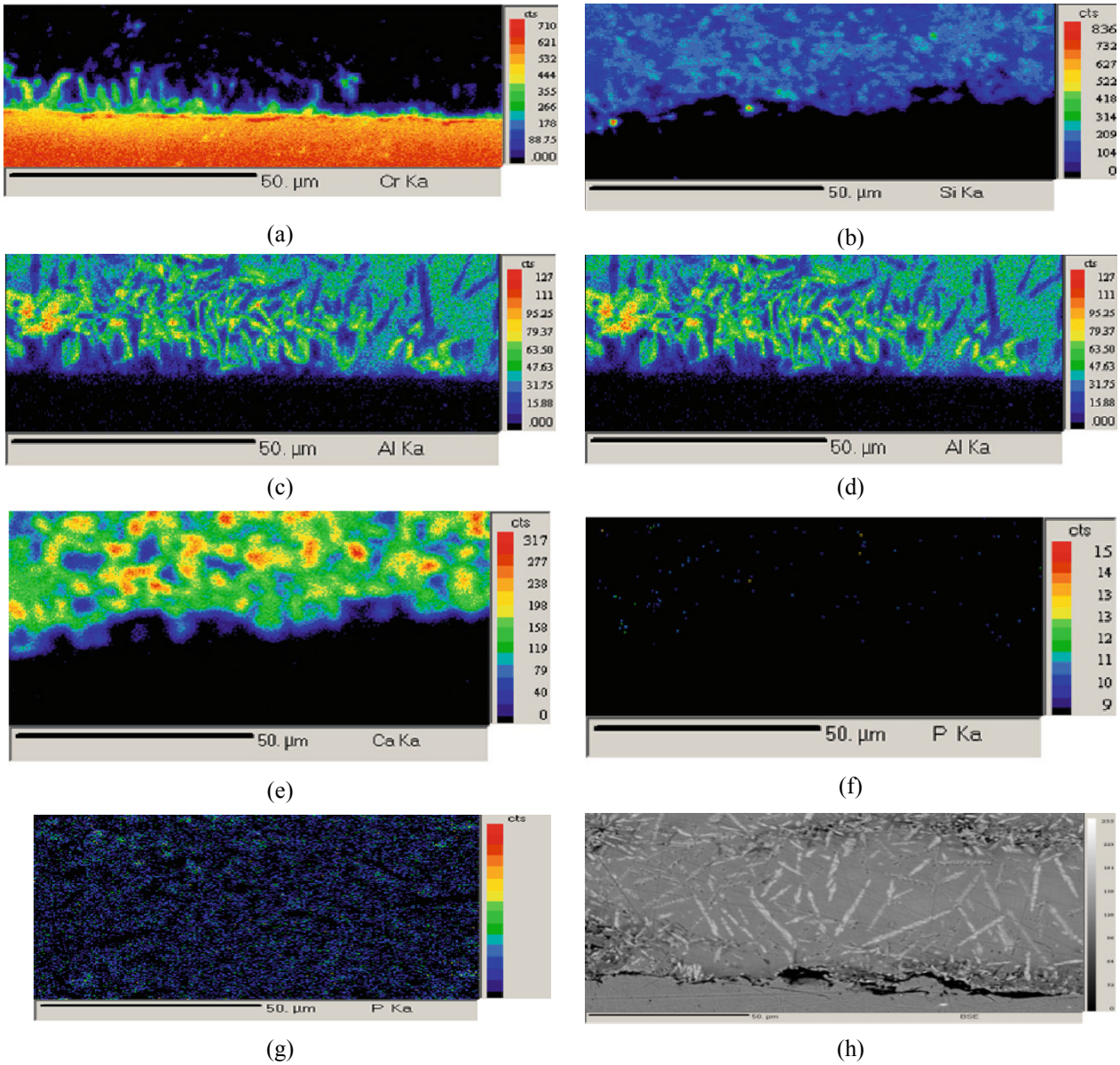

Fig. 13 Characteristic X-ray images of the BCABS-1P to Crofer 22 APU interface showing the distribution of (a) Cr, (b) Si, (c) Al, (d) Ba, (e) Ca, (f) P proximal to the interface, (g) P in the bulk of the glass-ceramic and (h) showing the microstructure at the interface with visible BaSiO3 dendrites

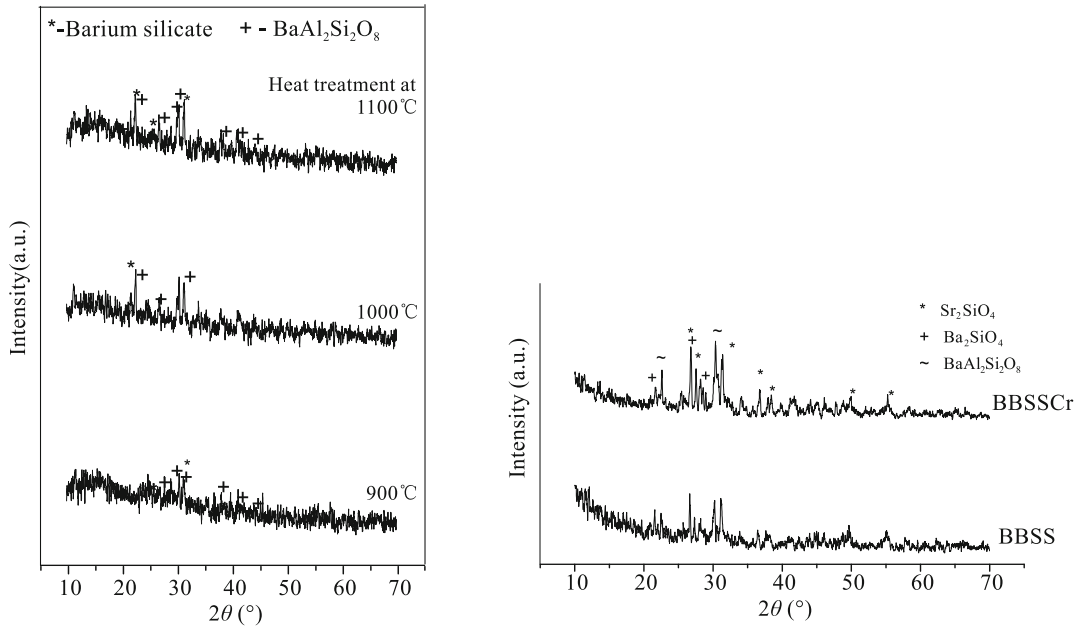

Fig. 14 (a) XRD plots of BSS after different heat treatment and (b) BBSS and BBSSCr after heat treatment 800 ℃ for 6 h

occurring at the glass-ceramic-to-metal interface, it is clear that either Reaction (3) or (4) would yield an interface saturated with metal ions. Since glass-to-metal bonding is enhanced by an interface saturated in metal ion, incorporation of P_2O_5 may improve adhesion [4].

It is also observed that despite P_2O_5 incorporation, diffusion of Cr^{3+} ions persists at the interface implying that $BaCrO_4$ formation continues to be an issue and this can be a limitation for applicability [43]. Incorporation of P_2O_5 into barium calcium aluminum borosilicate glass removes modifier cations from the silicate network, which leads an increased network polymerization. The consequences are the higher sintering temperatures and an increased crystallization tendency. The latter, allied with high sealing temperatures means that BCABS glass doping should be limited to up to 2 mol % P_2O_5. Above 2 mol % phase emergence changes from silicates to aluminosilicates and phosphates, which compromise the thermo-physical properties of the glass-ceramics. This implies that doping should be limited to 2 mol% P_2O_5 so that the major phase formed remains $BaSiO_3$ and the hexacelsian formation is minimized. However, at 2 mol% P_2O_5, incomplete sintering was evident in HSM measurements, due to rapid crystallization. Interface observations of glass-ceramics with Crofer alloy did not show any detrimental effect of P_2O_5, and bonding may even be enhanced by increased Cr diffusion. Therefore, we conclude that incorporation of 1 mol% P_2O_5 improves the sealing characteristics of BCABS glass-ceramics [39].

3 Sealants based on barium/strontiun zinc silicate (B/SZS) glass-ceramics

In order to evaluate the effect of La_2O_3 and Cr_2O_3 on glass properties and sealing behaviour, SrO/BaO based silicate glasses with these additives were prepared. Nominal compositions (in mole %) of the glass samples are listed in Table 4. The attendant changes in thermo-physical properties of the glasses are collated in Table 5. The T_g and TEC values reported in Table 5 are determined from TMA plots. The data presented in Table 5 indicates a reduction in T_g and an augmentation of TEC with incorporation of B_2O_3. The TEC values of the glass samples are found to be in the acceptable range for SOFC sealing.

Table 4 Nominal composition of glasses prepared with various additives

Sample	SiO_2	SrO	BaO	La_2O_3	Al_2O_3	B_2O_3	Cr_2O_3
BSS	38	20	30	0	10	0	2
BBSS	30	20	30	05	05	10	0
BBSSCr	30	20	30	05	05	8	2

Table 5 Thermo-physical properties of parent glasses

Sample	TEC (± 5%)(10^{-6}℃$^{-1}$)	T_g ±2(℃)
BSS	10.0	670
BBSS	11.4	650
BBSSCr	12.0	652

In glass and glass-ceramics, the thermo-physical properties are strongly dependent upon the composition [44,45]. In glasses, SiO_2 acts as network forming oxide [45]. Decreasing the silica content and increasing B_2O_3 reduces the rigidity of the glass network. Further, addition of Cr_2O_3 also contributes to decreasing network polymerization. Thus, the addition of B_2O_3 and Cr_2O_3 lead to an increase in the TEC of glasses, while T_g decreases.

XRD patterns of different glass samples after controlled heat treatment at different temperature are depicted in Fig. 14a. The BSS glass after heat treatment shows the formation of $BaSiO_3$ and $BaAl_2Si_2O_8$. However, the intensity of crystalline reflections is low implying the samples are not well crystallized. The others samples BBSS and BBSSCr showed comparatively good crystallization behaviour. XRD patterns of these glasses after controlled heat treatment at 800 ℃ (Fig. 14b) reveal the formation of Ba_2SiO_4, $BaAl_2Si_2O_8$and Sr_2SiO_4.

The glass transition temperature of glass corresponds to viscosity of $10^{11.3}$ Pa·s. Viscosity of the glass decreases with increasing temperature and significant wetting of metal is possible at higher temperature, where viscosity decreases to around 10^7-10^4 poise. Sealing of BSS glass with Crofer 22 APU alloy was possible at 1150-1200 ℃. However, for others composition satisfactory sealing is possible near 1000 ℃. The seals prepared with BBSS exhibits good bonding with metallic interconnect even after holding at 800 ℃ up to 500 h. Leak testing of seals were carried out and were found to withstand a vacuum of 10^{-6} Torr at room temperature.

4 Crystallization kinetics of SZS glasses

While BaO is a commonly used modifier in SOFC glasses, it leads to $BaCrO_4$ formation, which cannot be completely avoided owing to the highly negative Gibb's free energy of this phase at elevated temperatures, particularly in oxidizing environments [43]. Therefore, we investigate SrO containing silicates as potential sealant materials. It has been shown that incorporation of ZnO into strontium silicate glasses greatly mitigates the formation of $SrCrO_4$. Prolonged use of the silicate glass at elevated SOFC temperatures will lead to crystallization and conversion of the glass into a glass-ceramic. Therefore, it is of great importance to understand the crystallization kinetics of the SrO-ZnO-SiO_2 (SZS) glasses. Toward this, we performed DTA experiments on an SZS glass of composition (wt. %) 51SrO-9ZnO-40SiO_2 at heating rates ranging from 5-20 K·min^{-1} in an atmosphere of flowing Ar. We have discussed the details of the DTA measurements elsewhere [46]. The crystallization kinetics has been investigated using both the Kissinger [47] and Matusita-Sakka [48] methods. The latter method is needed because in the present glasses, there is a strong likelihood of nucleation occurring during crystal growth [48-50]. This situation will lead to an underestimation of the activation energy for crystallization derived from the Kissinger method, which assumes growth from a fixed number of nuclei [47-50]. The DTA curve on the SZS glass is presented in Fig. 15. It shows an endothermic event corresponding to T_g at nearly 700 ℃, while the a crystallization exotherm is evident at ~900 ℃. The exotherm was deconvoluted into two Gaussian peaks at 877 ℃ and 917 ℃ (Fig. 15). The position of these exotherms as a function of the heating rate is collated in Table 6. The activation energy was evaluated by the Kissinger equation and Matusita Sakka expression, the details of which we have discussed elsewhere [46].

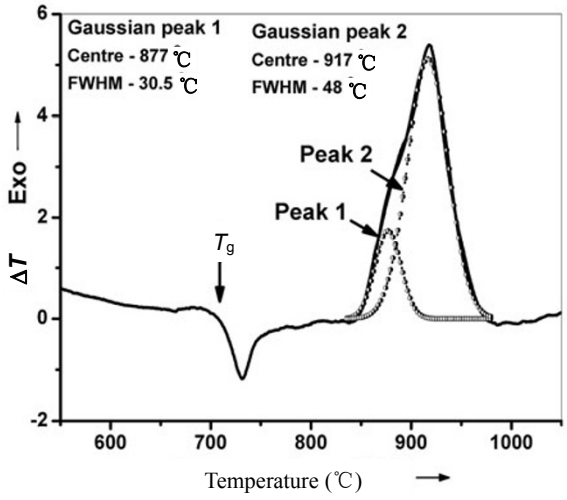

Fig. 15 DTA curve of the SZS glass at a heating rate of α=10 ℃/min

Table 6 Peak Temperatures of exotherms at different heating rates for the SZS glass

Heating rate (α) (℃/min)	T_{p1} (℃)	T_{p2} (℃)
5	860	896
10	877	917
15	889	929
20	895	942

The activation energy and crystallization growth parameters for the SZS glass are presented in Table 7. The values n and m presented in Table 7 indicate bulk crystallization with varying number of nuclei and diffusion controlled bulk crystallization [49,50]. The bulk crystallization is expected to proceed by 3 and 2 dimensional growth in case of peaks 1 and 2 respectively [48-50]. It is interesting to observe that if the activation energies obtained from the Kissinger method are corrected according to $E_a \approx (n/m)E_{ak}$ then there exists reasonable agreement between the activation energies measured by the Kissinger and Matusita-Sakka methods. Further, the activation energy obtained is quite high (Table 7) indicating thermally activated crystallization kinetics. The high crystallization temperature coupled with the diffusion dominated crystallization behaviour makes controlling the crystallization process more difficult.

Since two exotherms were evident in the DTA curve, crystallization of at least two phases is expected. Glasses were heat treated at different temperatures as shown in Table 8. Also presented in Table 8 are the phases realized upon heat treatment. The corresponding X-ray diffractograms are presented in Fig. 16. The samples heat treated at 720 ℃ for 1 h, 750 ℃ for 5 h and 820 ℃ for 1 h are amorphous. In the sample heat treated at 820 ℃ for 2 h, $ZnSiO_3$, SiO_2, Sr_2ZnSiO_2 and $Sr_3Si_3O_9$ are evident in the X-ray diffractograms (Fig. 17). In the glass sample heat treated at 850 ℃ for 2 h, the fraction of $ZnSiO_3$ and SiO_2 decreases in comparison to Sr_2ZnSiO_2 and $Sr_3Si_3O_9$. We postulate that $ZnSiO_3$ and SiO_2 are replaced by Sr_2ZnSiO_2 and $Sr_3Si_3O_9$ as the major phase according to the following reactions [46]:

$$SiO_2(\text{hexagonal})+SrO(\text{glass})\rightarrow SrSiO_3(\text{monoclinic})/Sr_3Si_3O_9 \quad (5)$$

$$ZnSiO_3(\text{orthorhombic})+2SrO(\text{glass})+SiO_2(\text{glass})\rightarrow Sr_2ZnSi_2O_7\ (\text{tetragonal}) \quad (6)$$

Table 7 Activation energy and growth morphology parameters for crystallization of the SZS glass

Sample	Peak	Average n (Ozawa)	m (Matusita)	E_{ak} (kJ/mol) (Kissinger)	E_a (kJ/mol) (Matusita)	(n/m) E_{ak} (kJ/mol)
SZS glass (75-200 μm particle size)	1	2.67 (~2.5)	1.5	409	700	681
	2	1.95 (~2)	1.0	342	704	684

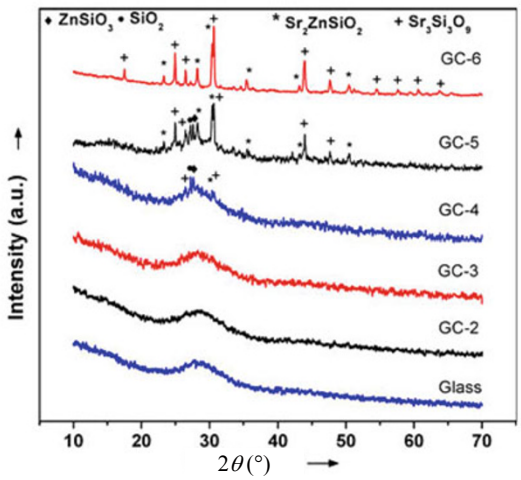

Fig. 16 Powder X-ray diffractograms of the SZS glass and glass-ceramics, produced by heat treatment of glass at different temperatures and for time durations

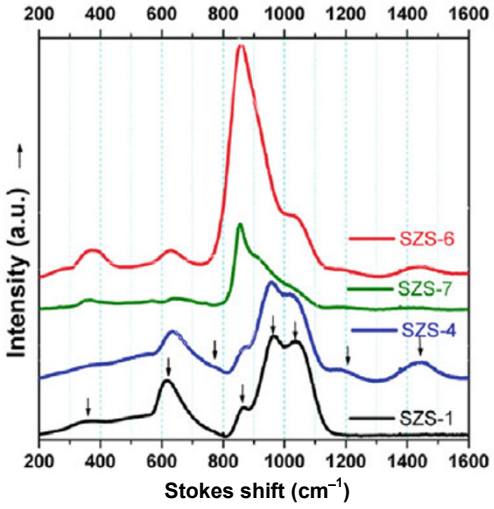

Fig. 17 Room temperature Raman spectra of investigated SZS glasses

Table 8 Heat-treatment schedules of the SZS glass-ceramics

Nomenclature	Heating temperature (℃)	Dwell time (h)	Crystalline phases
GC-1	750	1	Amorphous
GC-2	750	5	Amorphous
GC-3	820	1	Amorphous
GC-4	820	2	SiO_2, $ZnSiO_3$, $Sr_3Si_3O_9$, $Sr_2ZnSi_2O_7$
GC-5	850	2	Mainly $Sr_3Si_3O_9$, $Sr_2ZnSi_2O_7$ and minor quantity of SiO_2, $ZnSiO_3$
GC-6	925	2	$Sr_3Si_3O_9$, $Sr_2ZnSi_2O_7$

In the sample heat treated at 925 ℃, Sr_2ZnSiO_2 and $Sr_3Si_3O_9$ are the only phases detected on the X-ray diffractogram (Fig. 16). With increasing heat treatment temperature, the crystalline peaks in the X-ray diffractograms become more pronounced and the braod background attributed to the glassy phase decreases, indicating increasing crystallinity of the sample. Further, assuming all the ZnO in the glass participates in the formation of Sr_2ZnSiO_2 and all the SrO participates in the formation of Sr_2ZnSiO_2 and $Sr_3Si_3O_9$, we can estimate that the glass can reach at most ~87% crystallization. We can rule out further crystallization of SiO_2 based on the absence of more than 2 exotherms in DTA. The diffractogram of the glass treated at 925 ℃ shows high crystallinity and it appears that it has crystallized to near the maximum extent possible. However, we are pursuing long term heat treatment studies to verify that there is no further crystallization.

The SEM micrographs of the SZS glasses after being heat treated according to various schedules are presented in Fig. 18. The as prepared glass is completely uniform, testifying the homogeneity of the prepared glass (Fig. 18a). In the sample heat treated at 750 ℃ for 5 h, a vermicular phase separated structure is evident. It is likely that the SZS glass undergoes a glass in glass phase separation by the spinodal decomposition mechanism on the length scale of 50 -500 nm, leading to the characteristic connected morphology (Fig. 18b) [51]. Upon heat treating at 820 ℃, the phase separation, driven by the higher temperature becomes more evident and the boundaries between the phase separated regions become more distinct, growing to a length scale of 1-2 μm (Fig. 18c). In the sample heat treated at 850 ℃, which is close to the crystallization onset temperature (Fig. 15), the phase separated regions begin crystallizing and some granular/prismatic crystals about 2-4 μm in size are evident (Fig. 18d). These crystals are more numerous in the sample heat treated at 925 ℃ and the interconnected structure is very clearly evident for this sample (Fig. 18e). Also evident is the high crystallinity of the sample, confirming the X-ray diffractograms. The highly interconnected nature of the two phases clearly indicates the spinodal decomposition and phase separation occurs in the SZS glasses into regions rich in ZnO and regions rich in SiO_2 [51]. The ZnO rich regions crystallize to yield $Sr_2ZnSi_2O_7$, while $Sr_3Si_3O_9$ forms in the SiO_2 rich regions. Phase separation tendencies in binary SrO-SiO_2 [52] and ZnO-SiO_2 [53] systems are well known and it is therefore not really surprising that such behaviour persists in the ternary SZS glasses.

In the SZS glasses, the phase separation behaviour may lead to problems with degradation resistance particularly in the ZnO rich regions, which may persist for a longer time if the SOFC is operated at around 750-800 ℃. However, the rapid crystallization of SZS glasses to yield phases with acceptable TEC and stability is a major advantage. Further studies involving long durations of holding at elevated temperature are presently underway.

5 Effect of various additives in the SZS system

The glasses belonging to the SZS system have not been explored very commonly for sealing for SOFCs. In the previous section we discussed how the phase emergence behavior and crystallization kinetics of SZS glasses are promising for SOFC sealing applications. In this section, we discuss the effect of various additives such as B_2O_3, Al_2O_3, V_2O_5, and Cr_2O_3 in the SZS system [54]. The changes in the glass structure resulting from the composition modification were observed using Raman spectroscopy. The changes in phase emergence were studied using XRD and sealing studies with promising compositions was carried out to ensure that the SZS glasses show adequate bonding

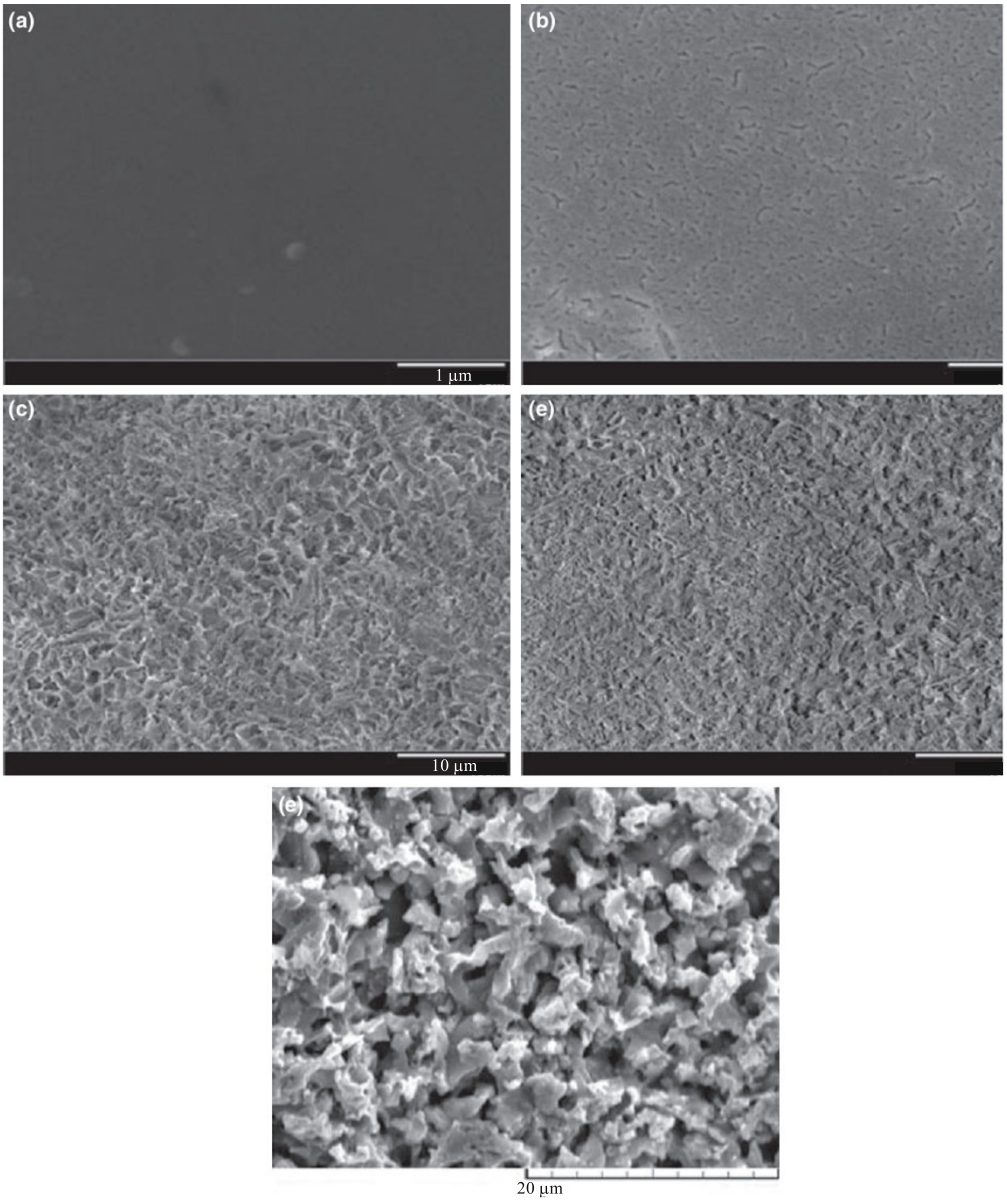

Fig. 18 SEM micrographs of the SZS glass and glass-ceramics (a) as-prepared glass, (b) glass-ceramic GC-2, crystallized at 750 ℃ for 5 h, (c) glass-ceramic GC-4, crystallized at 820 ℃ for 2 h, (d) glass-ceramic GC-5, crystallized at 850 ℃ for 2 h, and (e) glass-ceramic GC-6, crystallized at 925 ℃ for 2 h

characteristics with other SOFC components such as Crofer-22 APU and YSZ.

The compositions of the SZS glasses with various additives are presented in Table 9. Additives were added to modify the properties of the melt; Al_2O_3 for retarding crystallization, B_2O_3 for reducing sealing temperature and controlling viscosity. V_2O_5 and Cr_2O_3 were added to reduce surface tension of the glass/melt, which also act as nucleating agents in different glass compositions [39]. The details of glass preparation are discussed in the literature [54]. Various thermo-physical properties of glasses prepared are listed in Table 10.

Table 9 Chemical compositions (in wt. %) of investigated SZS glasses

Glass nomenclature	SrO	ZnO	SiO_2	B_2O_3	V_2O_5	Al_2O_3	Cr_2O_3
SZS-1	51	9	40	–	–	–	–
SZS-4	51	9	30	10	–	–	–
SZS-6	49	9	30	8	4	–	–
SZS-7	51	9	30	5	–	3	2

Table 10 Thermo-physical properties of investigated SZS glasses/glass-ceramics

Glass ID	T_g (℃)	T_{ds} (℃)	TEC (10^{-7}/℃)	T_{p1} (℃)	T_{p2} (℃)	MH (GPa)	Density (kg/m^3)	Major crystalline phases
SZS-1	722	745	108	890	930	6.26	3680	$Sr_2ZnSi_2O_7$, $SrSiO_3$
SZS-4	643	676	105	820	860	7.13	3710	$Sr_2ZnSi_2O_7$, $SrSiO_3$
SZS-6	640	664	115	830	–	7.17	3660	$Sr_2ZnSi_2O_7$
SZS-7	671	707	112	885	–	6.26	3780	$SrSiO_3$

The prepared glasses were bubble free, transparent and colourless except those having Cr_2O_3 or V_2O_5 oxides. Glasses having Cr_2O_3 were dark greenish in colour due to Cr^{3+} ions and glasses having V_2O_5 were light greenish in colour due to V^{3+} ions. Characteristic broad hump in powder XRD pattern confirmed the amorphous nature of the prepared glasses. It is clear from Table 10 that investigated glasses have density in the range of 3.66-3.78 g/cc and microhardness in the range of 6.26-7.17 GPa. Microhardness of all glasses was high, reflecting higher bond strength which increases penetration resistance during indentation [55]. Density of glass increases with addition of B_2O_3/Al_2O_3, since molecular weight of these oxides is higher as compared to molecular weight of SiO_2. However, density remains almost same with the addition of V_2O_5 along with B_2O_3 as for glass SZS-6. This can be explained on the basis of two opposing effects. Higher molecular weight of the constituent oxides increases the density. Simultaneously, an open glass network consisting of V_2O_5 decreases density.

DTA plots of investigated glasses are shown in Fig. 19. Endothermic base line shift indicates the glass transition and exotherm indicates the crystallization. It is clear from Fig. 19 that for glass SZS-1 exotherm is envelop of 2 overlapped peaks. Peak temperatures of these exotherms T_{p1} and T_{p2} are at around 890 ℃ and 930 ℃ respectively. Two exothermic peaks are corresponding to crystallization of two phases. Glass transition temperature and crystallization temperature reduces significantly with the addition of B_2O_3 for replacement of SiO_2. Since B_2O_3 reduces the viscosity of the glass thereby increases the diffusion of ions which, in turn, causes crystallization of glass at lower temperature. For glass SZS-4 two exothermic peaks are more broad and separated. As a consequence, overall intensity of these 2 peaks also decreases. These observations indicate that B_2O_3 suppress the crystallization tendency [56,57]. For glass SZS-6 broad exotherm at around 830 ℃ is observed. This revealed that V_2O_5 is not an effective nucleating agent in the investigated composition. For glass SZS-7 exotherm peak becomes very broad and shifts towards higher temperature at ~885 ℃. This shifting is due to the Al_2O_3 which retard the crystallization of the glass. Broadness of the exotherm indicates that Cr_2O_3 is not an effective nucleating agent in the investigated composition.

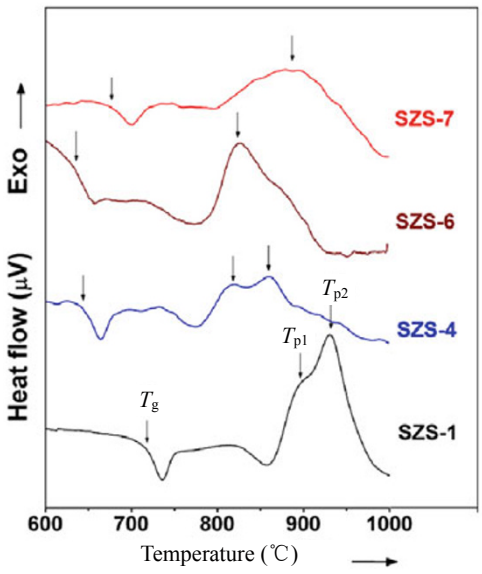

Fig. 19 DTA curve of investigated SZS glasses

It is observed that with the addition of B_2O_3, T_g and T_{ds} reduces and TEC remains almost unchanged. Since B_2O_3decrease the viscosity of the glass, it results in the reduction of T_g and T_{ds}. For glass SZS-6 addition of V_2O_5 also contributes in the reduction of T_g since V_2O_5 reduces the surface tension of liquid. Addition of V_2O_5 along with B_2O_3 increases the TEC of the glass. TEC for the investigated glasses are in the range of 105-115×10^{-7}/℃(30 ℃-T_g), which is closely matched with the TEC of other SOFC components like interconnect, electrodes and electrolytes [58,59]. It is found that TEC of glasses after 2 h crystallization did not change much (110-120×10^{-7}/℃). Softening temperature of all glass-ceramics is higher than 1000 ℃, which is advantageous for high temperature sealants. XRD spectra for different glass-ceramics are presented in Fig. 20. It is observed that for glass SZS-1 two crystalline phases $Sr_2ZnSi_2O_7$ and $SrSiO_3$ are formed, which correspond to 2 exothermic peaks in DTA data.

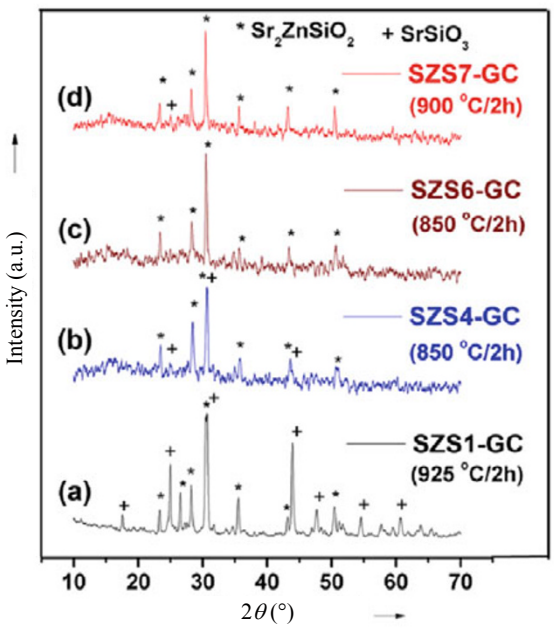

Fig. 20 Powder XRD spectra of SZS glass-ceramics (a) SZS1-GC crystallized at 925 ℃ for 2 h, (b) SZS4-GC crystallized at 850 ℃ for 2 h, (c) SZS6-GC crystallized at 850 ℃ for 2 h, (d) SZS7-GC crystallized at 900 ℃ for 2 h

For glass SZS-4 also both the phases crystallize but intensity of peaks corresponding to $SrSiO_3$ phase decreases which indicates the suppression of crystallization of this phase. For glass SZS-6 and SZS-7 mainly $Sr_2ZnSi_2O_7$ phase crystallized. XRD results indicate that in the base composition (SZS-1) $Sr_2ZnSi_2O_7$ and $SrSiO_3$ phases crystallize and addition of additives suppress the crystallization of $SrSiO_3$ phase, thus showing the presence of only $Sr_2ZnSi_2O_7$ phase. It is reported that glass ceramics containing crystalline phases of theses silicate groups have high thermal expansion coefficient [58].

Raman spectra of investigated glasses revealed the information regarding the modification in structure of glasses with the addition of other minor constitutes [56] as shown in Fig. 17. Bands in the 700-1100 cm^{-1} region are characteristic of Si-O^- stretching vibrations in different SiO_4 tetrahedron. Silica network is expressed in terms of Q^n structural units, where Q represents the Si tetrahedron and *n* the number of bridging oxygen per tetrahedron. For silica network *n* varies between 0 and 4. Raman spectrum of glass SZS-1 has intense bands at ~860, 940 and 1040 cm^{-1} and somewhat less intense, asymmetric band at ~620 cm^{-1} and a weak band at around 360 cm^{-1}. Based on the previous studies on silicate, borate and borosilicate glasses, bands at ~940 cm^{-1} and ~860 cm^{-1} are assigned to Si-O^- asymmetric stretching vibrations in Q^2 and Q^1 silicate structural units. Another band at around 1040 cm^{-1} is attributed to Si-O vibrations of bridging oxygen (Si-O-Si) in different Q^n silicate structural units. With the addition of other constituents, intensity of band at 860 cm^{-1} increases and intensity of band at 940 and 1040 cm^{-1} decreases. This indicates that Q^1 structural units are increasing and Q^2 structural units are decreasing in the glass network [60-63]. Weak broad band at ~360 cm^{-1} is attributed to rocking motion of silicate units and/or motion of cationic polyhedra [64]. New bands appeared in the Raman spectra of B_2O_3 containing glasses at ~1200 cm^{-1} and ~1450 cm^{-1}. Intensity of these bands increases as concentration of B_2O_3 increases. Bands at ~1200 cm^{-1} and ~1450 cm^{-1} are attributed to vibrations of B-O^- bond in triangular (BO_3) borate units [65-67]. The band appearing at ~780 cm^{-1} in spectra of glass SZS-4 is assigned to vibrations of B-O^- bonds in tetragonal (BO_4) borate units [65-67]. This indicates that initially B_2O_3 is going into the network as triangular (BO_3) borate units and at higher concentration of B_2O_3 (as in glass SZS-4) a part of the B_2O_3 only goes into the glass network as tetragonal (BO_4) borate units. Thus Raman spectra revealed that glass network mainly composed of Q^2 and Q^1 silicate structural units. With the addition of B_2O_3 and other additives silicate glass network depolymerizes and concentration of Q^1 structural units increases. These structural units are related to the crystalline phases of $Sr_2ZnSi_2O_7$ and $SrSiO_3$ developed in the glass matrix after heat treatment. It is known that generally Q^1 units [i.e., $(Si_2O_7)^{-6}$ dimers] constitute sorosilicate crystalline phases like $Sr_2ZnSi_2O_7$ and Q^2 structural units [i.e., $(SiO_3)^{-2}$] constitutes cyclosilicate and inosilicate phases like $SrSiO_3$ [68]. Thus structural study of glasses indicate that presence of silicate structural units in the glass network decide the formation of crystalline phases during heat treatment. Therefore, with the addition of additives as Q^1 units increases and Q^2 units decreases, only $Sr_2ZnSi_2O_7$ phase crystallize during heat treatment.

Adhesion behaviour of few glasses to YSZ was investigated. SEM image of the interface between YSZ and SZS-4 glass after heat treatment at 900 ℃ for 1 h in air ambient is shown in Fig. 21. Continuous interface shows good bonding between glass and YSZ. At interface elongated crystalline microstructure is also observed. Elemental line scans across interface (as presented in Fig. 21b) indicate that interdiffusion of Sr,

Si from glass side to YSZ side and interdiffusion of Y, Zr from YSZ side to glass side is responsible for good bonding with YSZ. It is found that interfacial zone is around 3-4 μm. Other investigated glasses have also shown good bonding with YSZ. Bonding behaviour of a few glasses with Crofer 22 APU was investigated. Figure 22a shows the SEM micrograph of the interface between Crofer 22 APU and SZS-6 glass after heat treatment at 950 ℃ for 1 h in air ambient. Smooth interface shows the good bonding between glass and Crofer 22 APU resulting from good wetting. Prismatic crystalline microstructure is observed at the interface. Interdiffusion of elements across the interface was observed through elemental line scans as presented in Fig. 22b. These indicate that interdiffusion of Cr, Fe from metal side to glass side and interdiffusion of Si from glass side to metal side takes place which is considered to be responsible for good bonding with Crofer 22 APU. Interfacial zone was found to be ~4 μm. Seals of SZS-6 glass with Crofer 22 APU were leak tested at different elevated temperatures up to 950 ℃ in the steps of 100 ℃, for 30 min at each temperature. Seals were found to withstand a vacuum of 10^{-6} torr in the whole temperature range. This indicates the leak tightness of the seal at high temperatures.

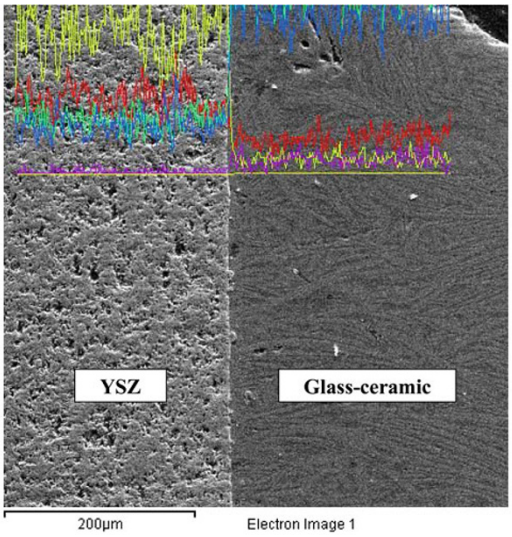

(a)

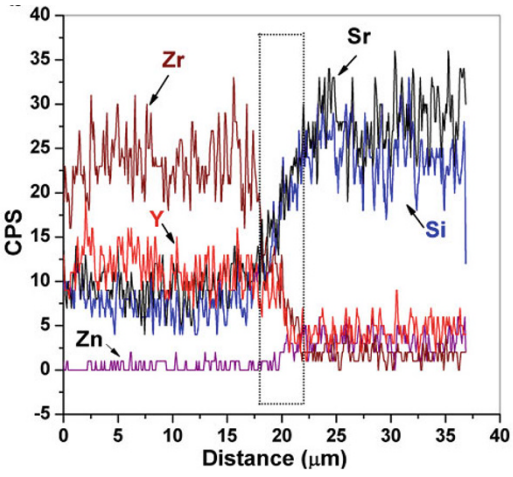

(b)

Fig. 21 (a) SEM micrographs of the SZS-4 glass-ceramic to YSZ interface after sealing at 950 ℃. (b) EDAX line scans across the interface showing the interdiffusion of Si, Sr, Zr and Y

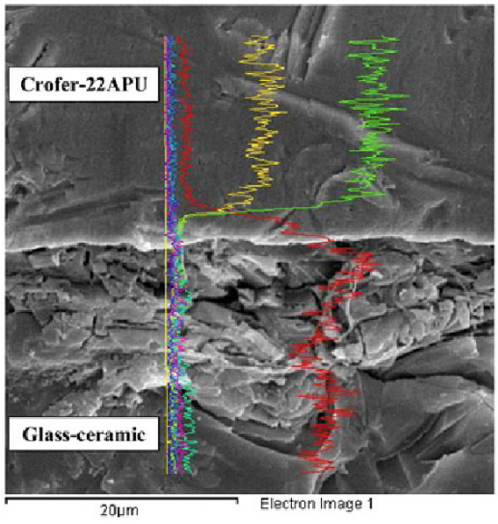

(a)

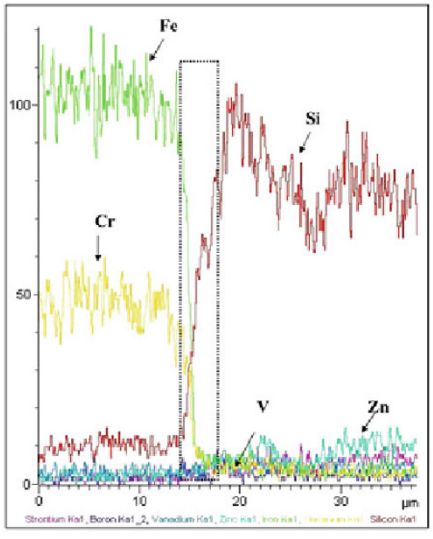

(b)

Fig. 22 (a) SEM micrographs of the SZS-6 glass-ceramic to Crofer 22 APU interface after sealing at 900℃. (b) EDAX line scans across the interface showing the interdiffusion of Fe, Cr and Si

6 Conclusions

We have systematically investigated glasses belonging to the BCABS and SZS systems as potential SOFC sealants. In case of the BCABS glasses, poor interaction with YSZ motivated the incorporation of additives in order to augment wetting and interface behaviour. P_2O_5 was found to be most suitable as an additive and 1 mole % P_2O_5 was found to be suitable for sealing. The incorporation of P_2O_5 helped in adhesion to Crofer-22 APU alloy by reaction with diffusing chromium leading to an interface saturated in Cr_2O_3. However, the problem of Cr diffusion and consequently the formation of $BaCrO_4$ in an oxygen rich environment persist.

In order to prevent/minimize chromate formation at the interface, SZS glasses were investigated. Using a combination of Kissinger and the Matusita-Sakka method, it is found that SZS glasses phase separate into SiO_2 and ZnO rich regions with $SrSiO_3$ and $Sr_2ZnSi_2O_7$ growing in these regions upon further heat treatment respectively. Upon further optimizing the SZS glasses using various additives, it is found that B_2O_3 allows a reasonable compromise between sealing properties, softening temperature and thermo-physical properties.

We are continuing to evaluate the properties of BCABS and SZS glasses with a focus upon long term stability, phase formation, interactions with other SOFC components and degradation behaviour under SOFC operating conditions. The studies carried out so far demonstrate the promise held by BCABS and SZS glass-ceramics as potential SOFC sealants and also the role played by complementary structural and thermo-physical characterization in optimizing properties of glasses and glass-ceramics for challenging applications such as high temperature SOFC sealing.

Acknowledgement

The authors thank the IFCPAR for funding this work vide project number 4008-1. The FEDER, Region Nord Pas-de-Calais, Ministère de l'Education Nationale de l'Enseignement Supérieur et de la Recherche, CNRS, and USTL are acknowledged for funding of NMR spectrometers. One of the authors (AA) thanks the DAE for awarding him a fellowship. The technical support of L Burylo, N Djelal, V Alaimo and S Bellayer is gratefully acknowledged.

References

[1] Ananthanarayanan A, Kothiyal GP, Montagne L, *et al*. MAS-NMR studies of lithium aluminum silicate (LAS) glasses and glass–ceramics having different Li_2O/Al_2O_3 ratio. *J Solid State Chem* 2010, **183**: 120-127.

[2] Ananthanarayanan A, Kothiyal GP, Montagne L, *et al*. MAS-NMR investigations of the crystallization behaviour of lithium aluminum silicate (LAS) glasses containing P_2O_5 and TiO_2 nucleants. *J Solid State Chem* 2010, **183**: 1416-1422.

[3] Ananthanarayanan A, Kumar R, Deo M N, *et al*. Preparation, structural and thermo-mechanical properties of lithium aluminum silicate glass-ceramics. *Ceram Int* 2009, **35**: 1661-1666.

[4] Donald IW. Glass-to-Metal Seals. Sheffield, UK: Society of Glass Technology, 2009.

[5] Barbieri L, Corradi AB, Leonelli C, *et al*. Effect of TiO_2 addition on the properties of complex aluminosilicate glasses and glass-ceramics. *Materials Research Bulletin* 1997, **32**: 637-648.

[6] Beall GH. Design and properties of glass-ceramics. *Annu Rev Mat Sc* 1992, **22**: 91-119.

[7] Best SM, Porter AE, Thian ES, *et al*. Bioceramics: Past present and for the future. *J Eur Ceram Soc* 2008, **28**: 1319-1327.

[8] Tumala RR. Ceramic and glass-ceramic packaging in the 1990s. *J Am Ceram Soc* 2005, **74**: 895-908.

[9] Kumar R, Arvind A, Goswami M, *et al*. The effect of NiO on the phase formation, thermo-physical properties and sealing behaviour of lithium zinc silicate glass-ceramics. *J Mater Sci* 2009, **44**: 3349-3355.

[10] Lee YK, Choi SY. Crystallization and properties of Fe_2O_3—CaO—SiO_2 glasses. *J Am Ceram Soc* 1996, **79**: 992-996.

[11] Sharma K, Dixit A, Bhattacharya S, *et al*. Effect of ZnO on phase emergence, microstructure and surface modifications of calcium phosphosilicate glass/glass-ceramics having iron oxide. *Applied Surface Sciences* 2010, **256**: 3107-3115.

[12] Sharma K, Singh S, Prajapat CL, *et al*. Preparation and study of magnetic properties of silico phosphate glass and glass-ceramics having iron and zinc oxide. *J Magnetism and Magnetic Materials* 2009, **321:** 3821-3828.

[13] Goswami M, Kothiyal GP, Montagne L, *et al*. MAS-NMR study of lithium zinc silicate glasses and glass-ceramics with various ZnO content. *J Solid State Chem* 2008, **181**: 269-275.

[14] Guo X, Sun K, Yan Y, *et al*. Investigation on silver

electric adhesive doped with Al_2O_3 ceramic particles for sealing planar solid oxide fuel cell. *J Power Sources* 2009, **192**: 408-413.

[15] Ley KL, Krumpelt M, Kumar R, *et al*. Glass-ceramic sealants for solid oxide fuel cells: Part I. Physical properties. *J Mater Res* 1996, **11**: 1489-1493.

[16] Mahapatra M K, Lu K. Glass-based seals for solid oxide fuel and electrolyzer cells—A review. *Mat Sci Eng R* 2010, **67**: 65-85.

[17] Mahapatra MK, Lu K, Jr WTR. Thermophysical properties and devitrification of $SrO–La_2O_3–Al_2O_3–B_2O_3–SiO_2$-based glass sealant for solid oxide fuel/electrolyzer cells. *J Power Sources* 2008, **179**: 106-112.

[18] Meinhardt KD, Kim DS, Chou YS, *et al*. Synthesis and properties of a barium aluminosilicate solid oxide fuel cell glass–ceramic sealant. *J Power Sources* 2008, **182**: 188-196.

[19] Menzler NH, Tietz F, Uhlenbruck S, *et al*. Materials and manufacturing technologies for solid oxide fuel cells. *J Mater Sci* 2010, **45**: 3109-3135.

[20] Singh RN. Sealing technology for solid oxide fuel cells (SOFC). *Int J Appl Cerm Technol* 2007, **4**: 134-144.

[21] Atkinson A, Sun B. Residual stress and thermal cycling of planar solid oxide fuel cells. *Mat Sci Tech* 2007, **23**: 1135-1143.

[22] Bao C, Shi Y, Li C, *et al*. Multi-level simulation platform of SOFC-GT hybrid generation system. *Int J Hydrogen Energy* 2010, **35**: 2894-2899.

[23] Hartman JS, Millard RL, Vance ER. A ^{29}Si magic angle spinning NMR study of vitreous and sol-gel precursors to sphene glass ceramics and their thermal crystallization. *J Non-Cryst Solids* 1989, **108**: 49-57.

[24] Kazeempur P, Dorer V, Ommi F. Evaluation of hydrogen and methane-fuelled solid oxide fuel cell systems for residential applications: System design alternative and parameter study. *Int J Hydrogen Energy* 2009, **34**: 8630-8644.

[25] Kendall K, Singhal SC, Minh NQ. Cell and Stack Design. 1st Ed. Amsterdam, the Netherlands: Elsevier, 2003.

[26] Larsen PH, James PF. Chemical stability of $MgO/CaO/Cr_2O_3–Al_2O_3–B_2O_3$–phosphate glasses in solid oxide fuel cell environment. *J Mater Sci* 1998, **33**: 2499-2507.

[27] Lee KH, Strand RK. SOFC cogeneration system for building applications, part 1: Development of SOFC system-level model and the parametric study. *Renewable Energy* 2009, **34**: 2831-2838.

[28] Lee KH, Strand RK. SOFC cogeneration system for building applications, part 2: System configuration and operating condition design. *Renewable Energy* 2009, **34**: 2839-2846.

[29] Al-Sulaiman FA, Dincer I, Hamdullahpur F. Exergy analysis of an integrated solid oxide fuel cell and organic Rankine cycle for cooling, heating and power production. *J Power Sources* 2010, **15**: 2346-2354.

[30] Bengisu MK, Brow RK, Yilmaz E, *et al*. Aluminoborate and aluminoborosilicate glasses with high chemical durability and the effect of P_2O_5 additions on the properties. *J Non-Cryst Solids* 2006, **352**: 3668-3676.

[31] Chang HT, Lin CK, Liu CK. Effects of crystallization on the high-temperature mechanical properties of a glass sealant for solid oxide fuel cell. *J Power Sources* 2009, **195**: 3159-3165.

[32] Fergus JW. Sealants for solid oxide fuel cells. *J Power Sources* 2005, **147**: 46-57

[33] Ghosh S, Sharma AD, Kundu P, *et al*. Development and characterizations of $BaO–CaO–Al_2O_3–SiO_2$ glass–ceramic sealants for intermediate temperature solid oxide fuel cell application. *J Non-Cryst Solids* 2008, **354**: 4081-4088.

[34] Lara C, Pascaul MJ, Prado MO, *et al*. Sintering of glasses in the system $RO-Al_2O_3$-BaO- SiO_2 (R=Ca, Mg, Zn) studied by hot-stage microscopy. *Solid State Ionics* 2004, **170**: 201-208.

[35] Ghosh S, Sharma AD, Kundu P, *et al*. Development and characterizations of $BaO-CaO-Al_2O_3-SiO_2$ glass-ceramic sealants for intermediate temperature solid oxide fuel cell application. *J Non-Cryst Solids* 2008, **354**: 4081-4085.

[36] Goel A, Tulyaganov DU, Pascaul MJ, *et al*. Development and performance of diopside based glass-ceramic sealants for solid oxide fuel cells. *J Non-Cryst Solids* 2010, **356**: 1070-1080.

[37] Wang SF, Wang YR, Hsu YF, *et al*. Effect of additives on the thermal properties and sealing characteristic of $BaO-Al_2O_3-B_2O_3-SiO_2$ glass-ceramic for solid oxide fuel cell application. *Int J Hydrogen Energy* 2009, **34**: 8235-8244.

[38] Sun T, Xiao H, Guo W, *et al*. Effect of Al_2O_3 content on $BaO-Al_2O_3-B_2O_3-SiO_2$ glass sealant for solid oxide fuel cell. *Ceram Int* 2010, **36**: 821-826.

[39] Ananthanarayanan A, Kothiyal GP, Montagne L, *et al*. The effect of P_2O_5 on the structure, sintering and sealing properties of barium calcium aluminum boro-silicate (BCABS) glasses. *Mater Chem Phys* 2011, **130**: 880-889.

[40] Caurant D, Majerus O, Loiseau P, *et al*. Crystallization of neodymium-rich phases in silicate glasses developed for nuclear waste immobilization.

J Nuclear Mat 2006, **354**: 143-162.

[41] Boccaccini AR, Hamann B. Review in Situ high-temperature optical microscopy. *J Mater Sci* 1999, **34**: 5419-5436.

[42] Mackenzie KJD, Kemmitt T. Evolution of crystalline aluminates from hybrid gel-derived precursors studied by XRD and multinuclear solid-state MAS NMR I. Celsian, $BaAl_2Si_2O_8$. *Thermochimica Acta* 1999, **325**: 5-12.

[43] Yang Z, Meinhardt KD, Stevenson JW. Chemical compatibility of Barium-Calcium-Aluminosilicate-based sealing glasses with the ferritic stainless steel interconnect in SOFCs. *J Electrochemical Soc* 2003, **150**: A1095-A1101.

[44] MacMillan PW. Glass-Ceramics. London, UK: Academic Press, 1979.

[45] Shelby JE. Introduction to Glass Science and Technology. Cambridge, UK: RSC, 2005.

[46] Tiwari B, Dixit A, Pillai CGS, *et al*. Crystallization kinetics and mechanism of strontium zinc silicate glass. *J Am Ceram Soc* 2012, **95**:1290-1296.

[47] Kissinger HE. Variation of peak temperature with heating rate in differential thermal analysis. *J Res Nat Bur Stand* 1956, **57**: 217-221.

[48] Matusita K, Sakka S. Kinetic study on crystallization of glass by differential thermal analysis criterion on application of Kissinger plot. *J Non-Cryst Solids* 1980, **38-39**: 741-746.

[49] Matusita K, Komatsu T, Yokota R. Kinetics of non isothermal crystallization process and activation energy for crystal growth in amorphous materials. *J Mater Sci* 1984, **19**: 291-296.

[50] Matusita K, Miura K, Komatsu T. Kinetics of non isothermal crystallization of some fluorozirconate glasses. *Thermochim Acta* 1985, **88**: 283-288.

[51] Mazurin OV, Porai-Koshits EA. Phase Separation in Glass. Amsterdam, the Netherlands: North-Hollan Physics Publishers, 1984.

[52] Huntelaar ME, Cordfunke EHP, Scheele A. Phase relations in the Strontium Oxide-Silica-Zirconium dioxide system I. The system $SrO\text{-}SiO_2$. *J Alloys Compd* 1993, **191**: 87-90.

[53] Ardit M, Cruciani G, Dondi M. The crystal structure of Sr-Hardystonite, $Sr_2ZnSi_2O_7$. *Z Kristallogr* 2010, **225**: 298-301.

[54] Tiwari B, Dixit A, Kothiyal GP. Study of glasses/ glass-ceramics in the $SrO\text{-}ZnO\text{-}SiO_2$ system as high temperature sealant for SOFC applications. *Int J Hydrogen Energy* 2011, **36**: 15002-15008.

[55] Rao KJ. Structural Chemistry of Glasses. Amsterdam, the Netherlands: Elsevier, 2002.

[56] Pascual MJ, Guillet A, Duran A. Optimization of glass-ceramic sealant compositions in the system MgO-BaO-SiO2 for solid oxide fuel cells (SOFC). *J Power Sources* 2007, **169**: 40-47.

[57] Harada T, Takebe H, Kuwabara M. Effect of B_2O_3 addition on the thermal properties and structure of bulk and powdered barium phosphate glasses. *J Am Ceram Soc* 2006, **89**: 247-250.

[58] Goel A, Pascual MJ, Ferreira JMF. Stable glass-ceramic sealants for solid oxide fuel cell. *Int J Hydrogen Energy* 2010, **35**: 6911-6923.

[59] Tietz F. Thermal expansion of SOFC materials. *Ionics* 1999, **5**: 129-139.

[60] Frantz JD, Mysen BO. Raman spectra and structure of $BaO\text{-}SiO_2$, $SrO\text{-}SiO_2$ and $CaO\text{-}SiO_2$ melts to 1600°C. *Chem Geol* 1995, **121:** 55.

[61] Roy BN. Spectroscopic analysis of the structure of silicate glasses along the joint $xMAlO_2\text{-}(1-x)SiO_2$ (M = Li, Na, K, Rb, Cs). *J Am Ceram Soc* 1987, **70:** 183.

[62] Kamitsos EI, Kapoutsis JA, Jain H, *et al*. Vibrational study of the role of trivalent ions in sodium trisilicate glass. *J Non-Cryst Solids* 1994, **171**: 31-45.

[63] Lin SL, Hawang CS. Structure of $CeO_2\text{-}Al_2O_3\text{-}SiO_2$ glasses. *J Non-Cryst Solids* 1996, **202**: 61-67.

[64] Tiwari B, Pandey M, Sudarsan V, *et al*. Study of structural modification of sodium aluminophosphate glasses with TiO_2 addition through Raman and NMR spectroscopy. *Physica B* 2008, **404**: 47-51.

[65] Chryssikos GD. Bond length-Raman frequency correlation in borate crystals. *J Raman Spectrosc* 1991, **22**: 645-650.

[66] Kamitsos EI, Karakassides MA, Chryssikos GD. Structure of borate glasses, part I: Raman study of cesium, rubidium and potassium borate glasses. *Phys Chem Glasses* 1989, **30**: 229-234.

[67] Raluca CL, Ioan A. FTIR and Raman study of silver lead borate based glasses. *J Non-Cryst Solids* 2007, **353**: 2020-2024.

[68] Holland W, Beall G. Glass-Ceramic Technology. Westerville, USA: The American Ceramics Society, 2002.